

FreRA: A Frequency-Refined Augmentation for Contrastive Learning on Time Series Classification

Tian Tian
tian006@e.ntu.edu.sg
Alibaba-NTU Singapore Joint
Research Institute, Interdisciplinary
Graduate Programme, Nanyang
Technological University
Singapore

Chunyan Miao
ascymiao@ntu.edu.sg
College of Computing and Data
Science, Nanyang Technological
University
Singapore

Hangwei Qian
qian_hangwei@cfar.a-star.edu.sg
CFAR, A*STAR
Singapore

Abstract

Contrastive learning has emerged as a competent approach for unsupervised representation learning. However, the design of an optimal augmentation strategy, although crucial for contrastive learning, is less explored for time series classification tasks. Existing predefined time-domain augmentation methods are primarily adopted from vision and are not specific to time series data. Consequently, this cross-modality incompatibility may distort the semantically relevant information of time series by introducing mismatched patterns into the data. To address this limitation, we present a novel perspective from the frequency domain and identify three advantages for downstream classification: 1) the frequency component naturally encodes *global* features, 2) the orthogonal nature of the Fourier basis allows *easier isolation* and *independent modifications* of critical and unimportant information, and 3) a *compact* set of frequency components can preserve semantic integrity. To fully utilize the three properties, we propose the lightweight yet effective **Frequency-Refined Augmentation (FreRA)** tailored for time series contrastive learning on classification tasks, which can be seamlessly integrated with contrastive learning frameworks in a plug-and-play manner. Specifically, FreRA automatically separates critical and unimportant frequency components. Accordingly, we propose semantic-aware Identity Modification and semantic-agnostic Self-adaptive Modification to protect semantically relevant information in the critical frequency components and infuse variance into the unimportant ones respectively. Theoretically, we prove that FreRA generates semantic-preserving views. Empirically, we conduct extensive experiments on two benchmark datasets, including UCR and UEA archives, as well as five large-scale datasets on diverse applications. FreRA consistently outperforms ten leading baselines on time series classification, anomaly detection, and transfer learning tasks, demonstrating superior capabilities in contrastive representation learning and generalization in transfer learning scenarios across diverse datasets. The code is available at <https://github.com/Tian0426/FreRA>.

CCS Concepts

• **Computing methodologies** → **Temporal reasoning; Unsupervised learning; Learning settings; Neural networks.**



This work is licensed under a Creative Commons Attribution 4.0 International License.
KDD '25, Toronto, ON, Canada

© 2025 Copyright held by the owner/author(s).
ACM ISBN 979-8-4007-1454-2/2025/08
<https://doi.org/10.1145/3711896.3736969>

Keywords

time series classification, contrastive learning, automatic augmentation, self-supervised learning

ACM Reference Format:

Tian Tian, Chunyan Miao, and Hangwei Qian. 2025. FreRA: A Frequency-Refined Augmentation for Contrastive Learning on Time Series Classification. In *Proceedings of the 31st ACM SIGKDD Conference on Knowledge Discovery and Data Mining V.2 (KDD '25)*, August 3–7, 2025, Toronto, ON, Canada. ACM, New York, NY, USA, 16 pages. <https://doi.org/10.1145/3711896.3736969>

1 Introduction

Time series classification has been an essential problem in a wide range of applications, such as activity recognition [24], speech recognition [11], and industrial monitoring [7]. Despite the promising performance achieved by supervised methods [24], a large number of accurate labels are required to deliver good performance. However, label annotation for time series without human error is costly and time-consuming. This is because time series data are not intuitively recognizable or meaningful for humans, unlike images or language. Given the circumstance, contrastive learning has been attested as a compelling framework for representation learning in the absence of labels [20, 25]. Specifically, it learns to solve an instance discrimination pretext task [33] that aims to distinguish different samples (negative pairs) while keeping different views of the same sample (positive pairs) close, wherein different views are usually generated by a set of augmentation functions.

Despite the prevalence of contrastive learning [4, 10], its efficacy heavily relies on the proper selection of data augmentation [17, 27]. Existing works in time series contrastive learning often apply carefully hand-picked time-domain transformations such as jitter-and-scale and permutation-and-jitter [7]. However, these augmentations are mostly adopted from the vision domain and do not take the intrinsic characteristics of time series into consideration. Due to the unintuitive nature of time series, it becomes impractical to painlessly figure out semantically compromised augmented samples, unlike in vision. Additionally, predefined stochastic frequency-domain augmentations, such as phase-shift and augmentation in TF-C [40], introduce semantically irrelevant noise that disrupts the critical information. Moreover, frequency-based predefined augmentations, such as high-pass and low-pass filters, require prior knowledge, such as the effective bandwidth of a dataset, to determine the selection of appropriate augmentation functions. As prior knowledge is not always accessible in the contrastive learning paradigm, and the compromised semantics caused by the

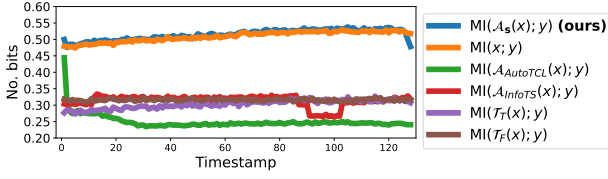


Figure 1: Our method (blue curve) achieves the highest MI between the views generated and the label, enabling better semantic preservation compared with SOTA. The semantically relevant information is well preserved to facilitate contrastive representation learning.

frequency-domain augmentation, predefined frequency-domain augmentations remain suboptimal for contrastive learning. Consequently, when applying predefined augmentation, the type and degree of transformation need to be carefully selected to reduce the loss of semantic information. However, the reliance on trial-and-error selection of hand-picked augmentations makes the process computationally expensive and impractical. What’s worse is that there is no single augmentation function that consistently performs well on all diverse datasets [25]. Given these challenges, recent works have started to explore the generalized principle and design of transformation that yield universally optimal augmentation v^* for time series contrastive learning. For instance, the latest InfoTS [17] and AutoTCL [41] share a common principle that optimal augmentation should remain semantically consistent with their anchor samples $MI(v^*; y) = MI(x; y)$, where x and y are the random variable denoting time series sample and *global* label applied to the entire sequence, and $MI(\cdot; \cdot)$ represents the mutual information (MI) quantifying the mutual dependence between two variables. MI is formally defined as $MI(x; y) = H(y) - H(y|x)$, where $H(y)$ and $H(y|x)$ denote the Shannon entropy of y and the entropy of y conditioned on x , respectively. However, our empirical observations reveal that these proposed augmentation strategies still fail to preserve semantic integrity. To be more specific, they more or less undermine or disrupt the meaningful patterns associated with semantically relevant information, i.e., $MI(v^*; y)$, of the time series, which will be discussed in detail in the later sections. In our analysis, the global semantics, whose amount is quantified as $MI(x; y)$, refer to *the information that spans the entire time series and contributes significantly to distinguishing between different classes*. Therefore, ensuring the preservation of global semantics is essential for effective view generation in contrastive learning for time series classification tasks.

For a clearer illustration, we plot 6 different $MI(v; y)$ curves in Figure 1, where $v \in \{A_s(x), x, A_{AutoTCL}(x), A_{InfoTS}(x), T_T(x), T_F(x)\}$, denoting the augmented view generated by our proposed FreRA, identity transformation, AutoTCL, InfoTS and jitter-and-scale and amplitude-and-phase-perturbation, respectively, and y is the label in the downstream classification task. The x -axis presents the timestamp of the time series, and the y -axis denotes the value of MI. We provide more details regarding Figure 1 in Appendix A.1. Intuitively, a higher MI curve is preferable because it indicates more global semantics information is preserved. We first observe the proposed FreRA (blue curve) achieves the highest value among all the curves, and it almost overlaps with $MI(x; y)$ (orange curve), indicating FreRA preserves all the semantically relevant information in the generated views and there is no major loss of critical information.

We then observe that the other four curves are consistently lower than the first two curves, indicating the semantically irrelevant information prevails and the global semantics are undermined in the latter three transformations, which agrees with our earlier analysis. Previous work [34] figures out that undermined semantics in the views cause degraded representation and harm the performance of downstream tasks, which is undesirable.

Despite strong empirical performance on certain datasets, existing augmentations introduce semantically irrelevant information which undermines semantically relevant context. This limitation highlights their inherent weaknesses. Due to the *inter-correlation among timestamps*, time-domain manipulations *fail to keep the critical global information intact while introducing variation*. Existing frequency-based augmentations do not fully leverage the advantages of the frequency domain. To address this gap, we reanalyze the frequency domain and identify 3 advantages of it over the time domain: 1) *global*: each frequency component encapsulates a global feature that spans all timestamps and is more meaningful in revealing the global semantics for classification tasks; 2) *independent*: the orthogonal Fourier basis ensures the independence among frequency components, making it unlikely to contain both critical and noisy information at the same time, which allows clear separation and independent manipulations on different components; and 3) *compact*: given the first two properties, there is a compactly distributed set of frequency components that can well preserve the semantic integrity, which reduces the risk of information loss while maintaining semantically relevant context. The three advantages of the frequency domain and how they facilitate the design of FreRA will be elaborated in detail in the latter sections.

To fully tap into the great potential of the frequency domain, we propose a novel **Frequency-Refined Augmentation (FreRA)** for contrastive learning on time series classification. The central idea of FreRA is to adaptively refine frequency components. Specifically, we learn a lightweight trainable parameter vector to capture the inherent semantic distribution in the frequency domain. Semantic-aware identity modification and semantic-agnostic self-adaptive modification are then proposed to the well-separated critical and unimportant frequency components respectively, to preserve global semantics and infuse variance. This single-parameter vector adeptly guides the refinement in both the separation and modifications. FreRA is a generalized transformation that automatically adapts to training data, alleviating manual efforts in adjusting augmentations. It also ensures that the added variation does not compromise the global semantics by refining the frequency domain rather than the time domain. FreRA can be easily adapted to a wide range of contrastive learning models in a plug-and-play manner. In summary, our main contributions are:

- We identify three advantages of the frequency domain and introduce the novel frequency perspective to automatic view generation for time series contrastive learning for the first time.
- Building upon these advantages, we design a lightweight and unified automatic augmentation FreRA for contrastive representation learning on classification tasks, which can be applied in a plug-and-play manner and jointly optimized with the contrastive learning model.

- Extensive experiments on 135 benchmark datasets demonstrate the competitive performance of FreRA in contrastive learning and improved generalization in transfer learning scenarios on both time series classification and anomaly detection tasks.

2 Related Work

Time series contrastive learning. Considering the challenges of data annotation for time series, contrastive learning achieves great success in time series applications [7, 19, 28, 38]. TS2Vec [38] performs hierarchical contrastive learning to learn timestamp-wise representations. TNC [28] learns temporal representations where neighboring and non-neighboring signals are distinguishable. TS-TCC [7] proposes a novel cross-view prediction task. MHCCL [19] utilizes hierarchical clustering for temporal contrastive representation learning. Although previous works introduce various architectures and objectives, the essence of contrastive learning lies in the attraction of positive pairs and the repulsion of negative pairs [9], making view generation a crucial component.

Frequency domain of time series. The frequency domain mostly serves as a substitute or supplementary modality in multiple time-series tasks, e.g., representation learning [35], domain generalization [40], and time series forecasting [37, 42, 43]. Those works empirically discover and exploit the frequency domain as an informative element: BTSF and TF-C [35, 40] encourage time-frequency consistency in representation learning to enhance generalization; Zhou et al. [42] claim that utilizing low-frequency Fourier components for time series forecasting could undermine noise; Zhou et al. [43] prove that a subset of randomly selected Fourier components preserves most of the information in the time series. Yi et al. [37] find that the frequency domain possessed a global view and compact energy in MLP-based time series forecasting. Those works provide heterogeneous understandings of identifying essential information in the frequency domain, either from domain knowledge or heuristics. In contrast, our motivation inspires a unified approach that manipulates frequency-domain information to facilitate contrastive learning. While predefined frequency-domain augmentations have been applied in time series contrastive learning [25, 40], the full potential of the frequency domain remains underutilized, leaving room for a more strategic augmentation approach.

Augmentations for contrastive learning. As a crucial component for contrastive learning, augmentation functions are either carefully designed or selected from grid search [7, 25]. The former requires domain knowledge, while the latter is computationally inefficient. There is no single existing augmentation function enjoying universal optimal performance [25]. The selection is task-dependent [27] and subject to data modality [12]. Some works try to automate the selection from a predefined set of transformations or adapt a well-defined transformation to serve contrastive learning: InfoTS [17] trains a data-driven probabilistic augmentation selector that intends to encourage high fidelity and variety to select optimal augmentation. Demirel and Holz [6] introduce tailored mixup for non-stationary quasi-periodic time series. Another line of work eliminates the use of hand-designed augmentation: InfoMin [27] generates contrastive views with a flow-based model, guided by the adversarial InfoMin objective. AutoTCL [41] factorizes the time

series instance to informative and noisy parts by timestamps. Self-adaptive augmentation in the frequency domain is less explored in contrastive learning, and we fill this research gap in this work.

3 Methodology

3.1 Problem Statement

Let $x = [x^1, x^2, \dots, x^L]^T \in \mathbb{R}^{L \times D}$ denote an unlabeled time series instance that lasts for L timestamps and has D channels where the signal at i -th timestamp $x^i \in \mathbb{R}^D, \forall i \in [1, \dots, L]$. We do not make assumptions about the dimension or length of the time series. Our problem definition is valid for both univariate and multivariate time series datasets of varying scales. $\mathcal{F}(\cdot)$ and $\mathcal{F}^{-1}(\cdot)$ represent the Fourier transform and its inverse, respectively. We denote $x_f = [x_f^1, x_f^2, \dots, x_f^F]^T = \mathcal{F}(x) \in \mathbb{C}^{F \times D}$ as the Fourier transform of x , i.e., $x = \mathcal{F}^{-1}(\mathcal{F}(x))$, where \mathbb{C} stands for the complex space and $F = \lfloor L/2 \rfloor + 1$ is the number of frequency components. x_f^1 and x_f^F embed the characteristics of the lowest and highest Fourier frequency basis functions, respectively.

In the general contrastive learning framework, an encoder f_θ is trained to map input samples to a latent space where the downstream task is performed. Taking SimCLR [3] as our contrastive learning framework, it appends a projector g_ϕ to the encoder. θ and ϕ denote the sets of trainable parameters in the encoder and projector respectively. In the mini-batch $X \in \mathbb{R}^{B \times L \times D}$ containing B instances, each anchor $x \in X$ associates with its augmented view $\mathcal{A}(x)$ as a positive pair, and with the other $(B - 1)$ samples to form negative pairs. We consider the batch-wise contrastive loss as: $\mathcal{L}_{\text{CL}} = \mathcal{L}(X; \mathcal{A}(\cdot), f_\theta, g_\phi)$, which will be elaborated later.

It is a common belief in existing works [17, 27, 41] that the optimal view generator for contrastive learning is defined as follows.

DEFINITION 1 (OPTIMAL VIEW GENERATOR). *Given the random variable x denoting the input instances, its optimal view generator $\mathcal{A}^*(\cdot)$ should satisfy $\mathcal{A}^*(x) = \arg \min_{\mathcal{A}} MI(\mathcal{A}(x); x)$, subject to $MI(\mathcal{A}^*(x); y) = MI(x; y)$.*

Based on the definition, an optimal view generator should preserve the *minimal but sufficient* information with respect to the global semantics of its input. Existing works on time series contrastive learning mainly select an empirically optimal augmentation function $\mathcal{T}^*(\cdot)$ from a set of predefined transformations $\{\mathcal{T}_1(\cdot), \mathcal{T}_2(\cdot), \dots, \mathcal{T}_m(\cdot)\}$, such as {scaling, jittering, rotation}, i.e.,

$$\mathcal{T}^*(\cdot), \theta^*, \phi^* = \arg \min_{\mathcal{T}_i(\cdot) \in \{\mathcal{T}_1(\cdot), \mathcal{T}_2(\cdot), \dots, \mathcal{T}_m(\cdot)\}, \theta, \phi} \mathcal{L}(X; \mathcal{T}_i(\cdot), f_\theta, g_\phi). \quad (1)$$

Selected from the painstaking trials and errors, $\mathcal{T}^*(\cdot)$ still suffers from loss of semantic information. Other works utilize a trainable network to model the transformation function, denoted as $\mathcal{T}(\cdot; \gamma)$, where γ is the parameters of the transformation network. They optimize the entire framework as follows:

$$\gamma^*, \theta^*, \phi^* = \arg \max_{\gamma} \arg \min_{\theta, \phi} \mathcal{L}(X; \mathcal{T}(\cdot; \gamma), f_\theta, g_\phi) + \mathcal{L}_{\text{auxiliary}}(\gamma), \quad (2)$$

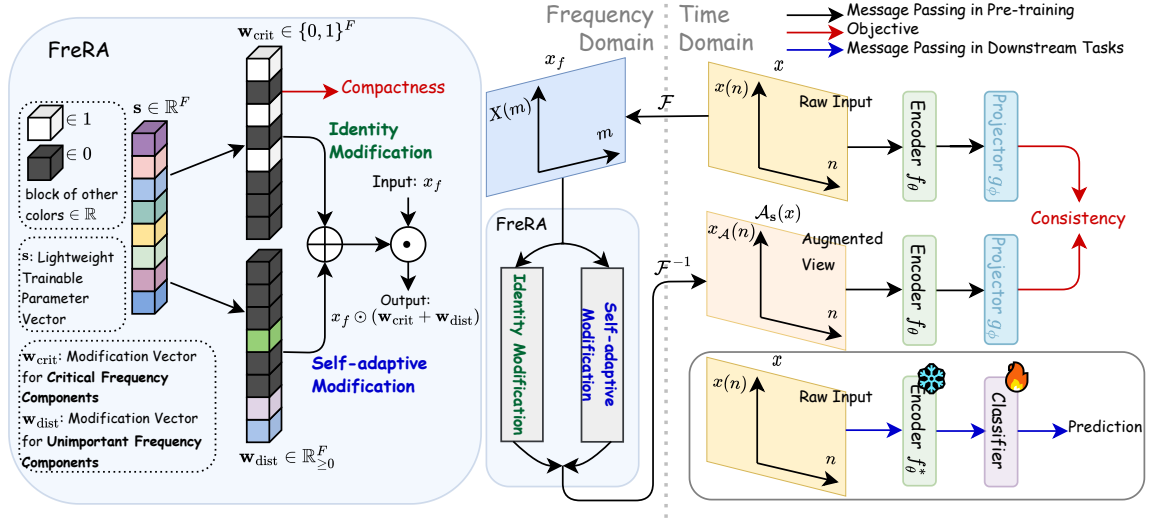


Figure 2: An overview of the proposed FreRA. The left-hand side presents the detailed design of FreRA: semantic-aware identity modification on critical components and semantic-agnostic self-adaptive modification on unimportant components are conducted in the frequency domain to maintain contextual information and infuse variance respectively. The matching colors between s and w_{dist} on unimportant components intend to illustrate the adaptive distortion. The independent manipulations in FreRA ensure the added variance does not impact the critical semantically relevant information. $X(m)$ and $x(n)$ represent the frequency domain and the time domain of time series respectively, where m denotes the index of frequency component and n denotes the timestamp index. As a plug-and-play component, FreRA can be jointly trained with any contrastive learning framework, as illustrated on the right-hand side. The contrastive learning model is pre-trained in the time domain. FreRA encourages the compactness of critical frequency components and the consistency of positive pairs' representations. In evaluation, a classifier is trained on top of the frozen pre-trained encoder to get predictions for downstream tasks.

where $\mathcal{T}(\cdot; \gamma^*)$ denotes the learned transformation function and $\mathcal{L}_{\text{auxiliary}}(\gamma)$ is the extra regularization on the transformation network. The optimization for the min-max objective is done through an alternative update of the transformation network and the contrastive learning model.

Aware of the selection cost, compromised semantics, and the complex alternative optimization in previous approaches, we aim to develop a semantic-preserving automatic augmentation $\mathcal{A}(\cdot)$ that can be jointly optimized with the contrastive learning model, with objective formulated as follows:

$$\begin{aligned} & \arg \min_{\mathcal{A}(\cdot), \theta, \phi} \mathcal{L}(X; \mathcal{A}(\cdot), \theta, \phi) + \mathcal{L}_{\text{auxiliary}}(\mathcal{A}(\cdot)) \\ & \text{subject to } \text{MI}(\mathcal{A}(x); y) = \text{MI}(x; y). \end{aligned} \quad (3)$$

In the following section, we will present the design of $\mathcal{A}(\cdot)$ and prove the fulfillment of Definition 1 as well as the criterion in the objective.

3.2 Overview of FreRA

It is a common belief that a good view in contrastive learning should contain both semantic-preserving information and a considerable amount of variance [17, 41]. The former ensures strong performance on downstream tasks, while the latter encourages the encoder to learn generalizable representations. To achieve such a good view, we leverage the global, independent, and compact properties of the frequency domain to design the frequency-refined augmentation,

FreRA as follows:

$$\mathcal{A}_s(x) = \mathcal{F}^{-1} \left(\underbrace{w_{\text{crit}} \odot x_f}_{\text{independent}} + \underbrace{w_{\text{dist}} \odot x_f}_{\text{global and compact}} \right) \in \mathbb{R}^{L \times D}, \quad (4)$$

where \odot denotes elementwise multiplication and s is the lightweight trainable parameter of FreRA. Specifically, $w_{\text{crit}} = [w_{\text{crit}}^1, w_{\text{crit}}^2, \dots, w_{\text{crit}}^F] \in \{0, 1\}^F$ applies semantic-aware identity modification on those identified critical frequency components to preserve the essential semantically relevant information, while $w_{\text{dist}} \in \mathbb{R}_{\geq 0}^F$ applies semantic-agnostic self-adaptive modification to the unimportant frequency components to introduce diverse distortion. The two modifications are applied independently to keep the critical global information intact while introducing variance. There may exist certain component x_f^i whose w_{crit}^i and w_{dist}^i are both 0. The refinement, including the component separation and modifications, is guided by a single vector s . Figure 2 depicts an overview of the proposed FreRA. Further details are elaborated in Section 3.3.

3.2.1 Why FreRA Makes Good Views? In this section, we elaborate the three advantages of the frequency domain over the time domain and elaborate on them in detail. Based on them, we explain why the frequency-domain refinement produces good views that benefit contrastive representation learning for downstream tasks. To facilitate our analysis, we introduce a new set of notation for time-domain data $x(n)$, augmented view $x_{\mathcal{A}}(n)$, and frequency-domain

data $X(m)$ as follows:

$$\begin{aligned} x(n) &= x^{n+1}, \quad x_{\mathcal{A}}(n) = \mathcal{A}_s(x^{n+1}) \quad \text{for } n \in \{0, 1, \dots, L-1\}, \\ X(m) &= \begin{cases} x_f^{m+1}, & \text{if } m+1 \leq F \\ \overline{X(L-m)} = \overline{x_f^{L-m+1}}, & \text{otherwise,} \end{cases} \quad \text{for } m \in \{0, 1, \dots, L-1\} \end{aligned} \quad (5)$$

where $\overline{x_f^{L-m+1}}$ is the conjugate of x_f^{L-m+1} , $x = [x(0), x(1), \dots, x(L-1)]^T$ and $x_f = [X(0), X(1), \dots, X(F-1)]^T$. We present the derivation for the second condition of $X(m)$ in Appendix A.2.1.

Global. The Fourier component is derived by Discrete Fourier Transform (DFT) [26]: $X(m) = \sum_{n=0}^{L-1} x(n)e^{-\frac{2\pi i}{L}mn}$, where each frequency component $X(m)$ encodes all the timestamps. According to the Dual convolution theorem [26], element-wise multiplication in the frequency domain is equivalent to circular convolution in the time domain. Then we have $\mathcal{F}(\tilde{\mathbf{w}} * x) = \frac{1}{F}\mathcal{F}(\tilde{\mathbf{w}}) \odot \mathcal{F}(x)$, where $*$ denotes the circular convolution operator. Let $\mathcal{F}(\tilde{\mathbf{w}}) = \mathbf{w}_{\text{crit}}$, we can conclude that the frequency modification is equivalent to time-domain convolution with kernel $\tilde{\mathbf{w}} = \mathcal{F}^{-1}(\frac{1}{F}\mathbf{w}_{\text{crit}}) \in \mathbb{C}^L$, which has global receptive field on x . This global perspective is crucial to the time series classification tasks, as it *preserves global semantics across the entire time series and ensures that all timestamps are altered with distortion applied only to unimportant components*.

Independent. The inverse DFT, $x(n) = \frac{1}{L} \sum_{m=0}^{L-1} X(m)e^{\frac{2\pi i}{L}mn}$, offers an alternative perspective of interpreting the frequency components: they are the coefficients of the orthogonal decomposition of the time domain. The decomposition basis for $X(m)$ is $\mathbf{u}_m = [e^{\frac{2\pi i}{L}mn} | n = 0, 1, \dots, L-1]^T \in \mathbb{C}^L$. We have $\langle \mathbf{u}_m, \mathbf{u}_q \rangle = 0$ if $m \neq q$, where $\langle \mathbf{u}, \mathbf{v} \rangle = \mathbf{u}^T \bar{\mathbf{v}} \in \mathbb{C}$ is the Hermitian inner product. The proof is presented in Appendix A.2.2. The zero-valued Hermitian inner product confirms the orthogonal nature of the decomposition basis. Each coefficient $X(m)$ measures the contribution of its corresponding basis function independently. Similarly, when FrERA modifies frequency components, each modified components independently contribute to the augmented views without being affected by the others. The independence *makes it easy to isolate critical and unimportant information* by updating \mathbf{w}_{crit} and \mathbf{w}_{dist} and prevent added variance from degrading critical information.

Compact. Parseval's theorem [22] states that the total energy of the signal in the time domain is equal to the average energy in the frequency domain, i.e., $\sum_{n=0}^{L-1} |x(n)|^2 = \frac{1}{L} \sum_{m=0}^{L-1} |X(m)|^2$. This implies that if most energy is concentrated in a small number of frequency components, the information of the signal is compactly distributed in the frequency domain. Figure 4 in the Appendix validates this interpretation by showing that most energy is concentrated on the first ten frequency components for the UCIHAR dataset and the same principle holds for other datasets. This aligns with our common sense that many natural or man-made processes recorded as time series encode information in low-frequency components. However, for classification tasks, the semantically relevant bandwidth is normally unknown and the importance of these components varies, making it hard to automatically rank their contributions and identify critical ones. Moreover, the exception happens in certain applications, such as audio processing [30], where both low- and high-frequency components matter. As critical components that encapsulate the semantically relevant information of the signal are

likely a subset of the compactly distributed informative components, their distribution should also remain compact. This leads us to *enforce compactness in identifying the critical components in the frequency domain*. Notably, the range of the energy in Figure 4 highlights the shared distribution of the informative components in the frequency domain. It advocates that a single vector \mathbf{s} is sufficient to work across all the samples in the dataset.

Lastly, we demonstrate that FrERA preserves global semantics of the time series, i.e., $\text{MI}(\mathcal{A}_s(\mathbf{x}); \mathbf{y}) = \text{MI}(\mathbf{x}; \mathbf{y})$ (Proposition 3 in the Appendix with proof) under the reliable assumption that noisy frequency components are independent to the label. This proposition agrees with our observation in Figure 1 where the blue and orange curves nearly overlap. It also shows that FrERA satisfies the semantic-preserving constraint in Definition 1, leaving only the minimization objective for optimization.

3.3 Time Series Contrastive Learning with FrERA

In this section, we first elaborate on the detailed design of FrERA and propose the objective that allows the joint training of FrERA and the contrastive learning framework.

Discern the importance of frequency components. Both \mathbf{w}_{crit} and \mathbf{w}_{dist} are parameterized by a lightweight trainable vector $\mathbf{s} = [s_1, s_2, \dots, s_F]^T \in \mathbb{R}^F$, where s_i scores the importance of the i -th frequency component x_f^i for the global semantics. A higher s_i indicates the contextual importance of x_f^i . On the other hand, s_i with a negative value suggests x_f^i is the noise component.

Semantic-aware identity modification on critical frequency components. A simple way to derive a binary vector like \mathbf{w}_{crit} is to sample from a Bernoulli distribution controlled by the parameter $\mathbf{p} = [p_1, p_2, \dots, p_F]^T \in \mathbb{R}^F$, i.e., $\mathbf{w}_{\text{crit}}^i \sim \text{Bernoulli}(p_i)$ for $i \in [1, 2, \dots, F]$, where p_i denotes the probability that the i -th frequency component is semantically critical. Meanwhile, the Bernoulli distribution is not differentiable w.r.t. p_i . Instead, we apply the Gumbel-Softmax reparameterization [13], i.e., $\mathbf{w}_{\text{crit}}^i = \text{Gumbel-Softmax}(p_i)$. The importance score vector \mathbf{s} makes it possible because its values can be used to reflect the probability, i.e., $p_i = \sigma(s_i)$, where $\sigma(\cdot)$ is the sigmoid function. The reparameterization is formulated as follows:

$$\mathbf{w}_{\text{crit}}^i = \sigma((\log \epsilon - \log(1 - \epsilon) + \log \frac{\sigma(s_i)}{1 - \sigma(s_i)}) / \tau_w), \quad (6)$$

where $\epsilon \sim \text{Uniform}(0, 1)$ and τ_w is the temperature controlling the discretization. As $\tau_w \rightarrow 0$, $\mathbf{w}_{\text{crit}}^i$ approximates a Bernoulli distribution: $P(\mathbf{w}_{\text{crit}}^i \rightarrow 0) = 1 - p_i$ if $\epsilon > p_i$, and $P(\mathbf{w}_{\text{crit}}^i \rightarrow 1) = p_i$ if $\epsilon < p_i$. In this way, distinct importance score s_i is assigned to x_f^i to capture varying levels of contextual relevance within each frequency component.

Semantic-agnostic self-adaptive modification on unimportant frequency components. Besides preserving contextually relevant information, a good view also requires variance to be infused. Instead of adding random noise, we deliberately modify the semantically irrelevant noisy components identified by \mathbf{s} to avoid affecting critical information. As the score s_i indicates the importance of the i -th frequency component x_f^i for global semantics, frequency components with smaller values are considered unimportant. A

threshold value is required to separate the unimportant components from the rest and handpicking such a value would be inefficient and troublesome due to its dataset-specific nature. A practical approach is to determine the value with statistical information of the vector. In this work, we use the mean value for convenience. We empirically compare the performance using alternative thresholds in Appendix A.6. Let $D = \{i | s_i < \min(0, \frac{1}{F} \sum_{i=1}^F s_i)\}$ denote the set of unimportant components' indices. Finding the minimum between the mean value and 0 ensures the threshold is non-positive. This is to prevent components with positive scores from being sampled. The distortion vector $\mathbf{w}_{\text{dist}} = \frac{1}{\delta_s} \mathbb{1}_{\{i \in D\}} \odot |\mathbf{s}| \in \mathbb{R}_{\geq 0}^F$ modifies the unimportant frequency components to various extent. The scaling factor $\delta_s = \frac{1}{|D|} \sum_{i=1}^F \mathbb{1}_{\{i \in D\}} |s_i|$ controls the degree of distortion such that it is in accordance to each component's insignificance and no dramatic interference will be introduced. Because of the absolute value function, the least important frequency component gets amplified mostly in the distortion step. Lastly, we apply stop-gradient operation, i.e., $\mathbf{w}_{\text{dist}} = \text{stopgrad}(\mathbf{w}_{\text{dist}})$ because back-propagation is not desired for the distortion. Data-driven thresholding and scaling define the self-adaptive nature of modification on semantically irrelevant frequency components. By modifying these components, variance is infused into all timestamps.

Overall objective. The Gumbel-Softmax reparameterization makes \mathbf{w}_{crit} differentiable, which allows the joint training of automatic augmentation and the contrastive learning framework. Specifically, the contrastive model is optimized by pulling positive pairs together and pushing negative pairs apart through the InfoNCE loss [29], given by:

$$\mathcal{L}_{\text{CL}} = -\frac{1}{B} \sum_{x \in X} \log \frac{\exp(\text{sim}(h_x, \hat{h}_x)/\tau)}{\sum_{x' \in X} \exp(\text{sim}(h_x, \hat{h}_{x'})/\tau)}, \quad (7)$$

where $h_x = g_\phi(f_\theta(x))$, $\hat{h}_x = g_\phi(f_\theta(\mathcal{A}_s(x)))$, $\text{sim}(\cdot, \cdot)$ denotes the similarity measurement implemented as the cosine similarity and τ is the temperature coefficient. Minimizing the InfoNCE loss is equivalent to maximizing the lower bound $\text{MI}_{\text{CL}}(x, \mathcal{A}_s(x))$ of the mutual information $\text{MI}(x, \mathcal{A}_s(x))$ [29], i.e., $\text{MI}(x, \mathcal{A}_s(x)) \leq \log(B) - \mathcal{L}_{\text{CL}} = \text{MI}_{\text{CL}}(x, \mathcal{A}_s(x))$, where B denotes the batch size. For $\mathcal{A}_s(\cdot)$, directly applying InfoNCE results in a trivial solution of \mathbf{s} that causes \mathbf{w}_{crit} to become an all-one vector $\mathbf{1} \in \{1\}^F$, leaving the importance of frequency components ambiguous. This is because $x = \mathcal{F}^{-1}(\mathbf{1} \odot x_f)$. On the other hand, the critical components should keep and only keep the semantically relevant information, as the name suggests, i.e., $\text{MI}(x_{\text{crit}}; x) = \text{MI}(x; y)$, where $x_{\text{crit}} = \mathcal{F}^{-1}(\mathbf{w}_{\text{crit}} \odot x_f)$. Knowing that DFT is a reversible operation, we prove $\text{MI}(x_{\text{crit}}; x) = \text{MI}(\mathbf{w}_{\text{crit}} \odot x_f; x_f)$ and $\text{MI}(x; y) = \text{MI}(x_f; y)$ in the Appendix A.3. The orthogonal property of the Fourier basis reminds us that the frequency components are uncorrelated. In other words, $\text{MI}(\mathbf{w}_{\text{crit}} \odot x_f; x_f)$ keeps increasing as a higher proportion of frequency components are identified as critical ones, as illustrated in Figure 5 in the Appendix, with proof provided in the Appendix A.3. The trivial solution falls on the right end of the red segment and the optimal proportion of critical components is pointed by the green arrow. To avoid the trivial solution and to achieve a good view, we regularize the proportion of critical components in complement to the InfoNCE loss. Specifically, we

employ the L1-norm on \mathbf{w}_{crit} as follows:

$$\mathcal{L}_{\text{reg}} = \frac{1}{F} \sum_{f=1}^F |\mathbf{w}_{\text{crit}}^f|. \quad (8)$$

The regularization eliminates redundancy from identifying too many critical frequency components, leading to compact selection and robust representation learning. The overall optimization problem is given by:

$$\mathbf{s}^*, \theta^*, \phi^* = \arg \min_{\mathbf{s}, \theta, \phi} (\mathcal{L}_{\text{CL}} + \lambda \cdot \mathcal{L}_{\text{reg}}), \quad (9)$$

where λ is a hyper-parameter to balance the two losses. Note that there exists a unique value of critical component's proportion that makes $\text{MI}(x_{\text{crit}}; x) = \text{MI}(x; y)$ happen, as shown in Figure 5. Meanwhile, as the hyper-parameter regularizes the proportion, λ empirically exhibits stable performance over a range of values, as shown in Figure 3.

How does the learning objective benefit view generation? Refining frequency components offers a key advantage in preserving global semantics, as each frequency component inherently encodes global information that spans the entire time series. Unlike time-domain augmentations, which disrupt inter-correlations among timestamps and compromise global semantics, FrERA leverages the global property of the frequency domain and independently modifies critical and unimportant components. This ensures that FrERA preserves global semantics while introducing proper variance. However, refining frequency components is inherently challenging due to the absence of ground truth labels, making it impractical to directly identify the optimal set of semantically relevant frequency components. Instead, FrERA relies on the contrastive learning objective to learn how to refine frequency components in a data-driven manner, effectively distinguishing between critical and unimportant information. From information theory, optimizing Eq. 9 is equivalent to maximize the lower bound for $\text{MI}(x, x_{\text{crit}})$ and minimize $\text{MI}(\mathcal{A}_s(x), x)$. The former occurs because optimizing \mathbf{s} over the InfoNCE loss only maximizes the lower bound for $\text{MI}(x, x_{\text{crit}})$, due to the stop-gradient operation applied to the unimportant frequency component. The latter is achieved by the regularization term and the distortion applied to unimportant components. Combined with the Proposition 3 we have proved earlier, we prove the view generator trained on objective in Eq. 9 satisfies the optimality as defined in Definition 1. Empirically, our results demonstrate that our proposed frequency-domain refinement significantly outperforms random sampling-based frequency modifications, validating the effectiveness of our approach in preserving global semantics while introducing meaningful variations.

Distinction to existing automatic augmentation for time series contrastive learning.

At first glance, our method may seem to resemble InfoTS [17], since it also leverages the same reparameterization trick to facilitate the view generation. However, their p_i indicates the probability of sampling a predefined transformation $\mathcal{T}_i(\cdot)$, i.e., $\mathcal{A}_{\text{InfoTS}}(x) = \frac{1}{m} \sum_{i=1}^m \text{Gumbel-Softmax}(p_i) \mathcal{T}_i(x)$. It fails to handle the noise and artifacts introduced by predefined augmentations $\mathcal{T}_i(\cdot)$. On the contrary, our approach elegantly eliminates the dependency on $\mathcal{T}_i(\cdot)$ by preserving critical elements and modifying the noise elements in the frequency domain. This more effectively enables preserving

Table 1: The overall performance on all the datasets (unit: %). best(T) and best(F) record the highest performances among the selected sets of 11 time-domain augmentations and 5 frequency-domain augmentations. The best performance is highlighted in bold, and the second-best performance is underlined. * indicates FreRA significantly outperforms both best(T) and best(F) at the confidence level of 0.05 from paired t-test.

Dataset	Metrics	FreRA (ours)	best(T)	best(F)	InfoMin ⁺	InfoTS	AutoTCL	TS2Vec	TNC	TS-TCC	TF-C	SoftCLT
UCIHAR	ACC	0.975*	0.959	0.960	<u>0.967</u>	<u>0.967</u>	0.697	0.959	0.568	0.924	0.875	0.961
MS	ACC	0.982*	0.956	0.970	<u>0.971</u>	0.967	0.691	0.945	0.526	0.915	0.811	0.962
WISDM	ACC	0.972*	0.942	0.950	<u>0.959</u>	0.915	0.760	0.939	0.543	0.889	0.839	0.952
UEA Archive	Avg. ACC	0.754*	0.684	0.686	0.693	0.714	0.742	0.704	0.670	0.668	0.298	<u>0.751</u> ¹
	Avg. RANK	2.133	5.967	5.800	5.500	3.967	<u>2.600</u>	4.967	6.433	6.033	9.276	-
UCR Archive	Avg. ACC	0.850*	0.723	0.744	0.718	<u>0.849</u>	0.598	0.845	0.776	0.780	0.542	0.850 ¹
	Avg. RANK	<u>1.940</u>	6.320	5.750	6.470	1.930	8.420	2.670	4.810	4.670	8.330	-

contextual-related information in the generated views while infusing variance. FreRA also appears similar to AutoTCL [41] in the sense that it disentangles the informative information of the time series from the noisy ones. However, performing the disentanglement on the time domain disrupts the periodicity and inter-dependencies among timestamps in the real world and hinders the semantics from the input space. Conversely, we disentangle the information in the frequency domain and leverage its advantages over the time domain: global, independent, and compact, to better facilitate the view generation.

4 Experiments

Datasets. To fully evaluate the model performance under different scenarios, we conduct extensive experiments on: (1) 3 large-scale datasets on HAR: UCIHAR [1], MotionSense (MS) [18], and WISDM [14]; (2) the UEA archive [2]: 30 multivariate time series datasets from various applications such as Human Activity Recognition (HAR), Motion classification, ECG classification, EEG/MEG classification, Audio Spectra Classification and so on; (3) the UCR archive [5]: 100 univariate time series datasets collected from real-world scenarios; (4) a large-scale anomaly detection dataset: Fault Diagnosis (FD) [16] aiming to detect and classify bearing damages from single-channel current signals of electric motors; (5) a large-scale HAR dataset for transfer learning scenario: SHAR [21], which contains daily activity signals from 30 persons and is empirically observed to have large distribution gap among individuals [25].

Baselines. We compare FreRA against the following related baselines: (1) 11 commonly-used handcrafted time-domain (T) augmentations [25], including jitter, scaling, negation, permutation, shuffling, time-flipping, time-warping, resampling, rotation, permutation-and-jitter, jitter-and-scale; (2) 5 handcrafted frequency-domain (F) augmentations [25], including low-pass filter, high-pass filter, phase shift, amplitude and phase perturbation (fully), and amplitude and phase perturbation (partially); (3) 3 SOTA automatic augmentation for contrastive learning: InfoMin [27], InfoTS [17], and AutoTCL [41]; (4) 5 SOTA time series contrastive learning frameworks: TS2Vec [38], TNC [28], TS-TCC [7], TF-C [40] and SoftCLT [15].

Implementation details. We use the predefined train-validation-test split if the dataset includes such information. Otherwise, we

split each dataset with a ratio of 64%:16%:20%. For time-series classification datasets with class imbalance issues, we sample training instances with probabilities inversely proportional to their class sizes. We implement FreRA in PyTorch [23] and conduct all experiments on an NVIDIA GeForce RTX 3090 GPU with 25 GB memory. Additional implementation details are included in Appendix A.4.

4.1 Main Results on Time Series Classification Tasks

The overall results on all the datasets are presented in Table 1. Overall, FreRA consistently outperforms all the baselines on the three large HAR datasets and achieves the top average accuracy and ranking on both UEA and UCR archives. The detailed performances of the UEA and UCR archives are reported in Table 9 and Table 8 in the Appendix. The critical difference diagrams on UEA and UCR archives are presented in Figure 7 in the Appendix. FreRA achieves the best performance on 17 out of 30 datasets in the UEA archive. We credit the surprising performance to the frequency-refined views generated by FreRA. The empirical performance adequately illustrates that FreRA can effectively keep the semantically relevant information from critical frequency components intact while infusing variance, boosting representation learning on all datasets. FreRA achieves leading performances not only on large-scale HAR datasets but also on extremely small datasets, e.g., AtrialFibrillation, DuckDuckGeese, and StandWalkJump within the UEA archive, whose training sets contain less than 100 samples, and the improvement over the second-best baselines is up to 8.7% on average. This is not only credited to the effectiveness of FreRA in maintaining semantics but also to the lightweight and scalable design where the number of parameters is only half of the sequence length. It also indicates that FreRA provides robust performance across datasets of varying sizes. Although FreRA achieves an average ranking 0.01 lower than InfoTS on the UCR archive, when comparing FreRA to the baselines of the same backbone structure, i.e. best(T), best(F) and InfoTS⁺, the improvement brought by the augmentation itself is significantly larger than the difference between InfoTS and TS2Vec. This indicates that FreRA offers stronger enhancement regardless of the backbone. We present a detailed analysis in the Appendix A.5.

Table 2: Performance on anomaly detection task on the Fault Diagnosis dataset. Each row corresponds to a setting where the pre-training set includes domains $\{a, bd, c\} \setminus \text{Target Domain}$, and the Target Domain is used for evaluation. The best accuracy is highlighted in bold, and the second-best performance is underlined.

Target Domain	Metrics	FreRA (ours)	best(T)	best(F)	InfoMin ⁺	InfoTS	AutoTCL	TS2Vec	TNC	TS-TCC	TF-C	SoftCLT
a	ACC	0.620	0.574	0.519	<u>0.613</u>	0.461	0.496	0.468	0.440	0.296	0.455	0.608
	Macro-F1	0.671	0.638	0.508	<u>0.644</u>	0.485	0.484	0.468	0.302	0.353	0.208	0.639
bd	ACC	0.859	<u>0.826</u>	0.767	0.807	0.731	0.433	0.802	0.455	0.823	0.455	0.808
	Macro-F1	0.895	<u>0.856</u>	0.817	0.853	0.798	0.471	0.848	0.300	0.755	0.208	0.853
c	ACC	0.819	0.810	0.736	<u>0.812</u>	0.742	0.482	0.677	0.465	0.557	0.455	0.775
	Macro-F1	0.858	0.794	0.755	<u>0.848</u>	0.781	0.456	0.747	0.314	0.617	0.208	0.825

Table 3: Classification performance in transfer learning setting on the SHAR dataset under different numbers of source domains. No. SD denotes the number of source domains for pre-training and TD denotes the index of the target domain. The best accuracy is highlighted in bold, and the second-best performance is underlined.

No. SD	TD	FreRA (ours)	best(T)	best(F)	InfoMin ⁺	InfoTS	AutoTCL	TS2Vec	TNC	TS-TCC	TF-C	SoftCLT
3	1	0.602	<u>0.599</u>	0.495	0.537	0.367	0.464	0.430	0.133	0.495	0.349	0.505
	2	0.467	<u>0.415</u>	0.412	0.359	0.369	0.278	0.317	0.145	0.410	0.252	0.407
	3	0.665	0.582	<u>0.599</u>	0.516	0.516	0.414	0.523	0.217	0.464	0.568	0.530
	5	0.366	0.332	0.336	0.359	0.081	0.245	0.050	0.143	<u>0.362</u>	0.255	0.339
19	1	0.628	0.555	<u>0.607</u>	0.542	0.599	0.497	0.568	0.117	0.578	0.453	0.581
	2	0.652	0.583	0.571	0.563	0.455	0.372	0.640	0.148	<u>0.647</u>	0.456	0.581
	3	0.691	0.628	<u>0.665</u>	0.638	0.563	0.408	0.502	0.135	<u>0.592</u>	0.451	0.559
	5	0.698	0.617	0.638	0.601	0.638	0.430	<u>0.658</u>	0.204	0.612	0.466	0.567

4.2 Evaluation on Anomaly Detection Tasks

We evaluate the performance of FreRA on the anomaly detection task using the Fault Diagnosis dataset and present the results in Table 2. The signals are collected under 4 different operation settings $\{a, b, c, d\}$. Observing the negligible domain gap between signals from settings ‘b’ and ‘d’, we randomly sample half of the data from each setting and combine them as a new domain ‘bd’. Considering the highly imbalanced class distribution, we include the Macro-F1 score as another evaluation metric. FreRA outperforms all the baselines on both evaluation metrics, which demonstrates its strong performance in applications beyond classification.

4.3 Evaluation on Transfer Learning

Here, we evaluate the generalizability of the pre-trained encoder, which is crucial when there exists a misalignment between the pre-training data and data from downstream tasks. The encoder is pre-trained on the source domains and adopted directly to an unseen target domain. Following [25], we conduct transfer learning in data-scarce and data-rich settings, where the number of source domains for training is 3 and 19 respectively. Table 3 records the results from the two settings. FreRA is shown to be more effective in learning generalizable encoders than all the baselines. This is because the views emphasizing the semantic-preserving patterns guide the training of the encoder and make it sensitive to the inherent global semantic information and robust to the semantically irrelevant information, i.e., distribution shift among different domains. Without effectively identifying critical and unimportant information, other SOTA baselines on automatic augmentation and time series contrastive learning fail to deliver promising performance in the transfer learning scenario.

4.4 Ablation Studies

Effect of each component. In Table 5, we evaluate the effect of each component of FreRA, i.e. the semantic-aware identity modification on critical frequency components, the semantic-agnostic self-adaptive modification on unimportant frequency components, and the regularization term. To disallow the identity modification on critical components, we randomly sample a proportion of critical components instead of identifying their distribution in a data-driven way. The proportion is the same as \mathcal{L}_{reg} from the last epoch of our approach to ensure fair comparison. To disallow the self-adaptive modification on unimportant frequency components, we set \mathbf{w}_{dist} as an all-zero vector. To ignore the regularization term, we let hyper-parameter λ be 0. Overall, removing any component deteriorates performance drastically. The semantic information and the distortion introduced are both crucial for downstream tasks. Between the two, the identity modification on critical components is slightly more important than the distortion on noisy components. It demonstrates the effectiveness of isolating critical and non-critical components from the frequency domain and applying the respective modifications accordingly. Last but not least, the L1-norm regularization is as crucial as the two frequency modification modules. The result demonstrates the importance of maintaining the inherent compact distribution of critical components.

Sensitivity to Hyper-parameter λ . Figure 3 shows the accuracy of FreRA on the 3 HAR datasets under varying λ compared to their second-best baselines plotted in dashed lines for reference. The result demonstrates that the downstream task performance remains stable across different values of λ and consistently better than the

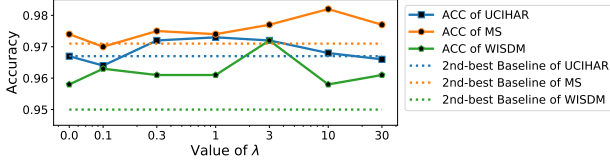
¹The result is directly adopted from its original paper. As the results across all the datasets in the UEA and UCR archives are not provided, the ranking is not available.

Table 4: The performance of the three large HAR datasets on alternative contrastive learning models.

Dataset	TS2Vec (InfoNCE)		TS-TCC (InfoNCE)		SoftCLT (InfoNCE)		SimCLR (InfoNCE)			SimCLR (NT-Xent)			BYOL (Cosine Similarity)		
	FrERA (ours)	original augmentation	FrERA (ours)	original augmentation	FrERA (ours)	original augmentation	FrERA (ours)	best(T)	best(F)	FrERA (ours)	best(T)	best(F)	FrERA (ours)	best(T)	best(F)
UCIHAR	0.970	0.959	0.944	0.924	0.969	0.961	0.975	0.959	0.960	0.972	0.951	0.955	0.960	0.940	0.937
MS	0.968	0.945	0.959	0.915	0.974	0.962	0.982	0.956	0.970	0.979	0.969	0.965	0.983	0.968	0.954
WISDM	0.957	0.939	0.962	0.889	0.956	0.952	0.972	0.942	0.950	0.966	0.941	0.952	0.952	0.942	0.928

Table 5: Effects of the two modification modules and the L1-norm regularization of FrERA. Results are averaged over 30 datasets from the UEA archive. The number in the bracket illustrates the accuracy gap with FrERA.

Methods	Avg. ACC
FrERA (ours)	0.754
w/o semantic-aware identity modification on critical components	0.690 (-0.064)
w/o semantic-agnostic self-adaptive modification on noise components	0.695 (-0.059)
w/o L1-norm regularization on \mathbf{w}_{crit}	0.690 (-0.064)

**Figure 3: Performance of FrERA on the 3 HAR datasets under varying λ , in comparison to their second-best baselines.**

baseline, indicating FrERA is robust to the selection of the hyper-parameter’s value. In Figure 3, UCIHAR, MS and WISDM achieve peak performances at $\lambda = 1, 10, 3$ respectively. On the left of the peak, the performance is suboptimal because redundant frequency components are included in the critical components. On the right of the peaks, incomplete critical information leads to degraded performances. The peak values indicate that FrERA learns to preserve only semantically relevant frequency components and distort the semantically irrelevant components, achieving the optimal view for representation learning.

On Alternative Contrastive Learning Frameworks. Due to its meticulous design, FrERA can be seamlessly integrated with different contrastive models in a plug-and-play manner. In Table 4, we apply FrERA to five alternative contrastive learning models: (1) three time-series contrastive models TS2Vec [39], TS-TCC [7], and SoftCLT [15] with their default augmentations as baselines and (2) two general purpose contrastive learning models originally designed for the vision domain, BYOL [8] and SimCLR [3] with the best time-domain and frequency-domain augmentations as baselines. For SimCLR, despite the NT-Xent loss originally applied in SimCLR, we also use InfoNCE as the loss function, which forms the framework we use in our main result. The same usage has been deployed in Yeh et al. [36] and Wu et al. [32] as well. Our current evaluation covers 5 contrastive learning frameworks and 3 types of contrastive loss functions. All the models differ in network design

and optimization objectives. It is worth noting that the contrastive losses used in TS-TCC, TS2Vec, and SoftCLT are different variants of InfoNCE, each with its unique formulation. The results presented consistently demonstrate that FrERA is a plug-and-play method that effectively enhances existing contrastive learning frameworks. This experiment highlights the flexibility and adaptability of our approach.

More comprehensive ablation studies investigating the effect of unimportant component selection mechanisms, and a case study on the learned vector \mathbf{s} are presented in the Appendix A.6.

5 Conclusion

In this paper, we propose Frequency-Refined Augmentation (FrERA), a lightweight yet effective automatic augmentation designed for time series contrastive learning on classification tasks. FrERA leverages the global, independent, and compact properties of the frequency domain to generate semantic-preserving views through independent modifications on separated frequency components. Its effectiveness is verified both theoretically and empirically. Experiments on 135 benchmark datasets across diverse applications demonstrate that FrERA is universally effective in contrastive learning and generalizes well in transfer learning scenarios. In addition, it is robust to hyper-parameter settings, flexible and effective when applied to various contrastive learning frameworks, and consistently able to capture the inherent semantically relevant information.

Acknowledgments

This research is supported by the RIE2025 Industry Alignment Fund – Industry Collaboration Projects (IAF-ICP) (Award I2301E0026), administered by A*STAR, as well as supported by Alibaba Group and NTU Singapore through Alibaba-NTU Global e-Sustainability CorpLab (ANGEL). Dr. Qian Hangwei is supported by A*STAR Career Development Fund <Project No. C243512010>.

References

- [1] Davide Anguita, Alessandro Ghio, Luca Oneto, Xavier Parra, and Jorge L Reyes-Ortiz. 2012. Human activity recognition on smartphones using a multiclass hardware-friendly support vector machine. In *Ambient Assisted Living and Home Care: 4th International Workshop, IWAAL 2012, Vitoria-Gasteiz, Spain. Proceedings* 4. Springer.
- [2] Anthony Bagnall, Hoang Anh Dau, Jason Lines, Michael Flynn, James Large, Aaron Bostrom, Paul Southam, and Eamonn Keogh. 2018. The UEA multivariate time series classification archive, 2018. *arXiv preprint arXiv:1811.00075* (2018).
- [3] Ting Chen, Simon Kornblith, Mohammad Norouzi, and Geoffrey E. Hinton. 2020. A Simple Framework for Contrastive Learning of Visual Representations. In *Proceedings of the 37th International Conference on Machine Learning, ICML 2020, Virtual Event (Proceedings of Machine Learning Research, Vol. 119)*. PMLR.
- [4] Xinlei Chen and Kaiming He. 2021. Exploring Simple Siamese Representation Learning. In *IEEE Conference on Computer Vision and Pattern Recognition, CVPR 2021, virtual*. Computer Vision Foundation / IEEE.
- [5] Hoang Anh Dau, Anthony Bagnall, Kaveh Kamgar, Chin-Chia Michael Yeh, Yan Zhu, Shaghayegh Gharghabi, Chotirat Ann Ratanamahatana, and Eamonn Keogh. 2019. The UCR time series archive. *IEEE/CAA Journal of Automatica Sinica* 6, 6 (2019).
- [6] Berken Utku Demirel and Christian Holz. 2024. Finding order in chaos: A novel data augmentation method for time series in contrastive learning. *Advances in Neural Information Processing Systems* 36 (2024).
- [7] Emadeldien Eldele, Mohamed Ragab, Zhenghua Chen, Min Wu, Chee-Keong Kwoh, Xiaoli Li, and Cuntai Guan. 2023. Self-supervised contrastive representation learning for semi-supervised time-series classification. *IEEE Transactions on Pattern Analysis and Machine Intelligence* 45, 12 (2023).
- [8] Jean-Bastien Grill, Florian Strub, Florent Altché, Corentin Tallec, Pierre Richemond, Elena Buchatskaya, Carl Doersch, Bernardo Avila Pires, Zhaohan Guo, Mohammad Gheshlaghi Azar, et al. 2020. Bootstrap your own latent—a new approach to self-supervised learning. *Advances in neural information processing systems* 33 (2020).
- [9] Kaiming He, Haoqi Fan, Yuxin Wu, Saining Xie, and Ross Girshick. 2020. Momentum contrast for unsupervised visual representation learning. In *Proceedings of the IEEE/CVF conference on computer vision and pattern recognition*.
- [10] Zhizhong Huang, Junping Zhang, and Hongming Shan. 2023. Twin Contrastive Learning with Noisy Labels. In *IEEE/CVF Conference on Computer Vision and Pattern Recognition, CVPR 2023, Vancouver, BC, Canada*. IEEE.
- [11] Iris AM Huijben, Arthur Andreas Nijdam, Sebastiaan Overeem, Merel M Van Gilst, and Ruud Van Sloun. 2023. Som-cpc: Unsupervised contrastive learning with self-organizing maps for structured representations of high-rate time series. In *International Conference on Machine Learning*. PMLR.
- [12] Ashish Jaiswal, Ashwin Ramesh Babu, Mohammad Zaki Zadeh, Debapriya Banerjee, and Fillia Makedon. 2020. A survey on contrastive self-supervised learning. *Technologies* 9, 1 (2020).
- [13] Eric Jang, Shixiang Gu, and Ben Poole. 2017. Categorical Reparameterization with Gumbel-Softmax. In *5th International Conference on Learning Representations, ICLR 2017, Toulon, France, Conference Track Proceedings*.
- [14] Jennifer R. Kwapisz, Gary M. Weiss, and Samuel Moore. 2010. Activity recognition using cell phone accelerometers. *SIGKDD Explor.* 12, 2 (2010).
- [15] Seunghan Lee, Taeyoung Park, and Kibok Lee. 2024. Soft Contrastive Learning for Time Series. In *The Twelfth International Conference on Learning Representations, ICLR 2024, Vienna, Austria*.
- [16] Christian Lessmeier, James Kuria Kimotho, Detmar Zimmer, and Walter Sextro. 2016. Condition monitoring of bearing damage in electromechanical drive systems by using motor current signals of electric motors: A benchmark data set for data-driven classification. In *PHM Society European Conference*, Vol. 3.
- [17] Dongsheng Luo, Wei Cheng, Yingheng Wang, Dongkuan Xu, Jingchao Ni, Wenchao Yu, Xuchao Zhang, Yanchi Liu, Yuncong Chen, Haifeng Chen, et al. 2023. Time series contrastive learning with information-aware augmentations. In *Proceedings of the AAAI Conference on Artificial Intelligence*, Vol. 37.
- [18] Mohammad Malekzadeh, Richard G. Clegg, Andrea Cavallaro, and Hamed Hadadadi. 2019. Mobile sensor data anonymization. In *Proceedings of the International Conference on Internet of Things Design and Implementation, IoTDI 2019, Montreal, QC, Canada*. ACM.
- [19] Qianwen Meng, Hangwei Qian, Yong Liu, Lizhen Cui, Yonghui Xu, and Zhiqi Shen. 2023. MHCCCL: masked hierarchical cluster-wise contrastive learning for multivariate time series. In *Proceedings of the AAAI Conference on Artificial Intelligence*, Vol. 37.
- [20] Qianwen Meng, Hangwei Qian, Yong Liu, Yonghui Xu, Zhiqi Shen, and Lizhen Cui. 2023. Unsupervised representation learning for time series: A review. *arXiv preprint arXiv:2308.01578* (2023).
- [21] Daniela Micucci, Marco Mobilio, and Paolo Napoletano. 2016. UniMiB SHAR: a new dataset for human activity recognition using acceleration data from smartphones. *abs/1611.07688* (2016). *arXiv:1611.07688*
- [22] Marc-Antoine Parseval. 1806. Mémoire sur les séries et sur l'intégration complète d'une équation aux différences partielles linéaires du second ordre, à coefficients constants. *Mém. prés. par divers savants, Acad. des Sciences, Paris*, (1) 1 (1806).
- [23] Adam Paszke, Sam Gross, Francisco Massa, Adam Lerer, James Bradbury, Gregory Chanan, Trevor Killeen, Zeming Lin, Natalia Gimelshein, Luca Antiga, et al. 2019. Pytorch: An imperative style, high-performance deep learning library. *Advances in neural information processing systems* 32 (2019).
- [24] Hangwei Qian. 2019. A Novel Distribution-Embedded Neural Network for Sensor-Based Activity Recognition (IJCAI-19). In *Proceedings of the 28th International Joint Conference on Artificial Intelligence (IJCAI), Macao, China*.
- [25] Hangwei Qian, Tian Tian, and Chunyan Miao. 2022. What Makes Good Contrastive Learning on Small-Scale Wearable-based Tasks?. In *KDD '22: The 28th ACM SIGKDD Conference on Knowledge Discovery and Data Mining, Washington, DC, USA*. ACM.
- [26] Duraismy Sundararajan. 2001. *The discrete Fourier transform: theory, algorithms and applications*. World Scientific.
- [27] Yonglong Tian, Chen Sun, Ben Poole, Dilip Krishnan, Cordelia Schmid, and Phillip Isola. 2020. What Makes for Good Views for Contrastive Learning?. In *Advances in Neural Information Processing Systems 33: Annual Conference on Neural Information Processing Systems 2020, NeurIPS 2020, virtual*.
- [28] Sana Tonekaboni, Danny Eytan, and Anna Goldenberg. 2021. Unsupervised Representation Learning for Time Series with Temporal Neighborhood Coding. In *9th International Conference on Learning Representations, ICLR 2021, Virtual Event, Austria*. OpenReview.net.
- [29] Aaron van den Oord, Yazhe Li, and Oriol Vinyals. 2018. Representation Learning with Contrastive Predictive Coding. *abs/1807.03748* (2018). *arXiv:1807.03748*
- [30] Tuomas Virtanen, Jort Florent Gemmeke, Bhiksha Raj, and Paris Smaragdis. 2015. Compositional models for audio processing: Uncovering the structure of sound mixtures. *IEEE Signal Processing Magazine* 32, 2 (2015).
- [31] Zhiguang Wang, Weizhong Yan, and Tim Oates. 2017. Time series classification from scratch with deep neural networks: A strong baseline. In *2017 International Joint Conference on Neural Networks, IJCNN 2017, Anchorage, AK, USA*. IEEE.
- [32] Junkang Wu, Jiawei Chen, Jiancan Wu, Wentao Shi, Xiang Wang, and Xiangnan He. 2024. Understanding contrastive learning via distributionally robust optimization. *Advances in Neural Information Processing Systems* 36 (2024).
- [33] Zhirong Wu, Yuanjun Xiong, Stella X. Yu, and Dahua Lin. 2018. Unsupervised Feature Learning via Non-Parametric Instance Discrimination. In *2018 IEEE Conference on Computer Vision and Pattern Recognition, CVPR 2018, Salt Lake City, UT, USA*. Computer Vision Foundation / IEEE Computer Society.
- [34] Jie Xu, Shuo Chen, Yazhou Ren, Xiaoshuang Shi, Hengtao Shen, Gang Niu, and Xiaofeng Zhu. 2024. Self-Weighted Contrastive Learning among Multiple Views for Mitigating Representation Degeneration. *Advances in Neural Information Processing Systems* 36 (2024).
- [35] Ling Yang and Shenda Hong. 2022. Unsupervised time-series representation learning with iterative bilinear temporal-spectral fusion. In *International Conference on Machine Learning*. PMLR.
- [36] Chun-Hsiao Yeh, Cheng-Yao Hong, Yen-Chi Hsu, Tyng-Luh Liu, Yubei Chen, and Yann LeCun. 2022. Decoupled contrastive learning. In *European conference on computer vision*. Springer.
- [37] Kun Yi, Qi Zhang, Wei Fan, Shoujin Wang, Pengyang Wang, Hui He, Ning An, Defu Lian, Longbing Cao, and Zhendong Niu. 2023. Frequency-domain mlps are more effective learners in time series forecasting. *Advances in Neural Information Processing Systems* 36 (2023).
- [38] Zhihan Yue, Yujing Wang, Juanyong Duan, Tianmeng Yang, Congrui Huang, Yunhai Tong, and Bixiong Xu. 2022. Ts2vec: Towards universal representation of time series. In *Proceedings of the AAAI Conference on Artificial Intelligence*, Vol. 36.
- [39] Zhihan Yue, Yujing Wang, Juanyong Duan, Tianmeng Yang, Congrui Huang, Yunhai Tong, and Bixiong Xu. 2022. Ts2vec: Towards universal representation of time series. In *Proceedings of the AAAI conference on artificial intelligence*, Vol. 36.
- [40] Xiang Zhang, Ziyuan Zhao, Theodoros Tsiligkaridis, and Marinka Zitnik. 2022. Self-supervised contrastive pre-training for time series via time-frequency consistency. *Advances in Neural Information Processing Systems* 35 (2022).
- [41] Xu Zheng, Tianchun Wang, Wei Cheng, Aitian Ma, Haifeng Chen, Mo Sha, and Dongsheng Luo. 2024. Parametric Augmentation for Time Series Contrastive Learning. In *The Twelfth International Conference on Learning Representations, ICLR 2024, Vienna, Austria*.
- [42] Tian Zhou, Ziqing Ma, Xue Wang, Qingsong Wen, Liang Sun, Tao Yao, Wotao Yin, and Rong Jin. 2022. FiLM: Frequency improved Legendre Memory Model for Long-term Time Series Forecasting. In *NeurIPS*.
- [43] Tian Zhou, Ziqing Ma, Qingsong Wen, Xue Wang, Liang Sun, and Rong Jin. 2022. FEDformer: Frequency Enhanced Decomposed Transformer for Long-term Series Forecasting. In *International Conference on Machine Learning, ICML 2022, Baltimore, Maryland, USA (Proceedings of Machine Learning Research, Vol. 162)*. PMLR.

A Appendix

A.1 Details regarding Figure 1

Directly calculating the mutual information between the entire time series and the label is not trivial due to the curse of dimensionality. To address this, in Figure 1, we calculate the mutual information between each timestamp and the label. It visualizes the amount of semantic information preserved across all the timestamps. For instance, the value of the orange curve at timestamp $\forall t \in [1, \dots, L]$ is $MI(x^t; y)$ of the UCIHAR dataset, where $x^t \in \mathbb{R}^D$ is the signal at timestamp t , y is the ground truth label. $L = 128$ and $D = 6$ are the length and dimension of the samples. Estimating the timestamp-wise mutual information, with a dimension of only 6, allows us to avoid the curse of dimensionality. In this plot, we do not intend to suggest a single timestamp alone is fully representative of the underlying semantics. Instead, the figure illustrates how the informative content varies across different augmentation functions. While a single timestamp may not directly indicate specific semantic meaning, the plot demonstrates the manipulation of the frequency domain benefits the augmented views. This is attributed to the undeteriorated critical components that are semantically informative.

A.2 Properties of the Discrete Fourier Transform (DFT)

A.2.1 Conjugate Symmetric. Given a signal $x(n) \in \mathbb{R}, n \in \{0, 1, \dots, L-1\}$, its DFT $X(m) \in \mathbb{C}, m \in \{0, 1, \dots, L-1\}$ is conjugate symmetric, i.e., $X(L-m) = \overline{X(m)}$. The proof is as follows:

$$\begin{aligned} X(L-m) &= \sum_{n=0}^{L-1} x(n) e^{-\frac{2\pi i}{L}(L-m)n} \\ &= \sum_{n=0}^{L-1} x(n) e^{\frac{2\pi i}{L}mn} \\ &= \overline{X(m)}. \end{aligned} \quad (10)$$

Converting back to our notation, $X(m) = \overline{X(L-m)} = x_f^{L-m+1}$, which explains the second condition of $X(m)$ in Eq. 5. The Conjugate Symmetry allows only half of the DFT signal to recover the entire time series, which also justifies why FreRA manipulates only half of the frequency components, i.e., $F = \lfloor L/2 \rfloor + 1$. This property allows FreRA to have a lightweight structure.

A.2.2 Orthogonal of Fourier basis. The inverse DFT, i.e.,

$$x(n) = \frac{1}{L} \sum_{m=0}^{L-1} X(m) e^{\frac{2\pi i}{L}mn}, \quad (11)$$

decompose the time domain on the Fourier basis $\mathbf{u}_m = [e^{\frac{2\pi i}{L}mn}]_{n=0, 1, \dots, L-1}^T \in \mathbb{C}^L$, where frequency components $X(m)$ are the coefficients with respect to the Fourier basis. The orthogonal property of Fourier basis, i.e., $\langle \mathbf{u}_m, \mathbf{u}_q \rangle = 0$ if $m \neq q$, is proved below.

$$\begin{aligned} \langle \mathbf{u}_m, \mathbf{u}_q \rangle &= \mathbf{u}_m^T \overline{\mathbf{u}_q} \\ &= \sum_{n=0}^{L-1} e^{\frac{2\pi i}{L}mn} e^{-\frac{2\pi i}{L}qn} \\ &= \sum_{n=0}^{L-1} e^{\frac{2\pi i}{L}(m-q)n} \\ &= \sum_{n=0}^{L-1} r^n = \frac{1-r^L}{1-r} \quad (12) \end{aligned}$$

(the sum of a geometric series follows: $\sum_{n=0}^{L-1} r^n = \frac{1-r^L}{1-r}$)

$$\begin{aligned} &= \frac{1 - e^{\frac{2\pi i}{L}L(m-q)}}{1 - e^{\frac{2\pi i}{L}(m-q)}} \\ &= \frac{e^{\frac{2\pi i}{L}L(m-q)} - 1}{e^{\frac{2\pi i}{L}(m-q)} - 1} \text{ if } m \neq q \\ &= 0 \end{aligned}$$

A.3 Proofs of Propositions

PROPOSITION 1. (Conservation of Entropy) Let x and x_f be the random variables denoting the time series in the time domain and the frequency domain respectively, then we have $H(x) = H(x_f)$.

PROOF. Since the DFT is a one-to-one invertible transformation, we have $p(x) = p(x_f)$.

$$\begin{aligned} H(x) &= \sum_x p(x) \log p(x) \\ &= \sum_{x_f} p(x_f) \log p(x_f) \\ &= H(x_f) \end{aligned} \quad (13)$$

□

PROPOSITION 2. (Conservation of Mutual Information) Let x , x_f , and y be the random variables denoting the time series in the time domain and the frequency domain, and their corresponding label respectively, then we have $MI(x; y) = MI(x_f; y)$.

PROOF. Since the DFT does not alter the label of the time series variable, we have $p(x, y) = p(x_f, y)$.

$$\begin{aligned} MI(x; y) &= H(y) - H(y|x) \\ &= H(y) - \sum_{x, y} p(x, y) \log \frac{p(x, y)}{p(x)} \\ &= H(y) - \sum_{x_f, y} p(x_f, y) \log \frac{p(x_f, y)}{p(x_f)} \\ &= MI(x_f; y) \end{aligned} \quad (14)$$

Similarly, we can proof $MI(x; \tilde{x}) = MI(x_f; \tilde{x}_f)$, where random variable x and \tilde{x} denotes two time series and x_f and \tilde{x}_f denotes their frequency-domain counterpart. □

PROPOSITION 3. With the reliable assumption that the noisy frequency components are independent to the label, FreRA is a semantic preserving transformation, i.e., $MI(\mathcal{A}_s(x); y) = MI(x; y)$.

PROOF. Let $\mathbf{x}_f^{\text{crit}} = \mathbf{w}_{\text{crit}} \odot \mathbf{x}_f$ and $\mathbf{x}_f^{\text{dist}} = (\mathbf{1} - \mathbf{w}_{\text{crit}}) \odot \mathbf{x}_f$ denote the critical and noisy frequency components respectively. Knowing $\mathbf{x}_f^{\text{crit}}$ and $\mathbf{x}_f^{\text{dist}}$ are independent, we have

$$H(\mathbf{x}_f) = H(\mathbf{x}_f^{\text{crit}}) + H(\mathbf{x}_f^{\text{dist}}). \quad (15)$$

Then we show that

$$\begin{aligned} \text{MI}(\mathbf{x}_f; \mathbf{y}) &= H(\mathbf{x}_f) - H(\mathbf{x}_f; \mathbf{y}) \\ &= H(\mathbf{x}_f^{\text{crit}}) + H(\mathbf{x}_f^{\text{dist}}) - H(\mathbf{x}_f^{\text{crit}}, \mathbf{x}_f^{\text{dist}} | \mathbf{y}) \\ &\quad (\mathbf{x}_f^{\text{dist}}, \text{ as irrelevant components, is independent to } \mathbf{y}) \\ &= H(\mathbf{x}_f^{\text{crit}}) + H(\mathbf{x}_f^{\text{dist}}) - (H(\mathbf{x}_f^{\text{crit}} | \mathbf{y}) + H(\mathbf{x}_f^{\text{dist}})) \\ &= H(\mathbf{x}_f^{\text{crit}}) - H(\mathbf{x}_f^{\text{crit}} | \mathbf{y}) \\ &= \text{MI}(\mathbf{x}_f^{\text{crit}}; \mathbf{y}). \end{aligned} \quad (16)$$

Similarly,

$$\begin{aligned} \text{MI}(\mathcal{A}_s(\mathbf{x}); \mathbf{y}) &= \text{MI}((\mathbf{w}_{\text{crit}} + \mathbf{w}_{\text{dist}}) \odot \mathbf{x}_f; \mathbf{y}) \\ &= H((\mathbf{w}_{\text{crit}} + \mathbf{w}_{\text{dist}}) \odot \mathbf{x}_f) - H((\mathbf{w}_{\text{crit}} + \mathbf{w}_{\text{dist}}) \odot \mathbf{x}_f; \mathbf{y}) \\ &= H(\mathbf{w}_{\text{crit}} \odot \mathbf{x}_f) + H(\mathbf{w}_{\text{dist}} \odot \mathbf{x}_f) \\ &\quad - H((\mathbf{w}_{\text{crit}} \odot \mathbf{x}_f + \mathbf{w}_{\text{dist}} \odot \mathbf{x}_f) | \mathbf{y}) \\ &\quad (\mathbf{w}_{\text{dist}} \odot \mathbf{x}_f \text{ is independent to } \mathbf{y}) \\ &= H(\mathbf{x}_f^{\text{crit}}) + H(\mathbf{w}_{\text{dist}} \odot \mathbf{x}_f) - (H(\mathbf{x}_f^{\text{crit}} | \mathbf{y}) + H(\mathbf{w}_{\text{dist}} \odot \mathbf{x}_f)) \\ &= H(\mathbf{x}_f^{\text{crit}}) - H(\mathbf{x}_f^{\text{crit}} | \mathbf{y}) \\ &= \text{MI}(\mathbf{x}_f^{\text{crit}}; \mathbf{y}). \end{aligned} \quad (17)$$

Applying Proposition. 2, we have $\text{MI}(\mathcal{A}_s(\mathbf{x}); \mathbf{y}) = \text{MI}(\mathbf{x}; \mathbf{y})$. \square

PROPOSITION 4. $\text{MI}(\mathbf{w}_{\text{crit}} \odot \mathbf{x}; \mathbf{x})$ is monotonically increasing w.r.t the proportion of critical components.

PROOF.

$$\begin{aligned} \text{MI}(\mathbf{w}_{\text{crit}} \odot \mathbf{x}_f; \mathbf{x}_f) &= H(\mathbf{x}_f) - H(\mathbf{x}_f | \mathbf{w}_{\text{crit}} \odot \mathbf{x}_f) \\ &= H(\mathbf{x}_f) - H(\mathbf{w}_{\text{crit}} \odot \mathbf{x}_f, (\mathbf{1} - \mathbf{w}_{\text{crit}}) \odot \mathbf{x}_f | \mathbf{w}_{\text{crit}} \odot \mathbf{x}_f) \\ &\quad (\mathbf{w}_{\text{crit}} \odot \mathbf{x}_f \text{ and } (\mathbf{1} - \mathbf{w}_{\text{crit}}) \odot \mathbf{x}_f \text{ are independent} \\ &\quad \text{since they lie on the orthogonal basis}) \\ &= H(\mathbf{x}_f) - H((\mathbf{1} - \mathbf{w}_{\text{crit}}) \odot \mathbf{x}_f) \\ &= H(\mathbf{x}_f) - \sum_{i=1}^F \mathbb{1}_{\{1 - \mathbf{w}_{\text{crit}}^i = 1\}} H(\mathbf{x}_f^i) \end{aligned} \quad (18)$$

Since the first term $H(\mathbf{x}_f)$ is fixed, and the second term decreases as the proportion of critical components increases, we prove the monotonic increasing of $\text{MI}(\mathbf{w}_{\text{crit}} \odot \mathbf{x}_f; \mathbf{x}_f)$ w.r.t the proportion of critical components. As the proportion becomes 1, i.e., all the frequency components are identified as critical ones, $\text{MI}(\mathbf{w}_{\text{crit}} \odot \mathbf{x}_f; \mathbf{x}_f) = H(\mathbf{x}_f)$, as we plot in Figure 5. \square

A.4 Implementation Details

For the predefined time-domain and frequency-domain augmentations, we follow the parameter settings from [25]. For the InfoMin baseline, we apply its adversarial objective to replace our regularization term. To make it suitable for time series, we use our frequency-domain refinement to substitute the flow-based view generator which is designed for images. This implementation makes it benefit from our frequency-enhanced approach and we denote

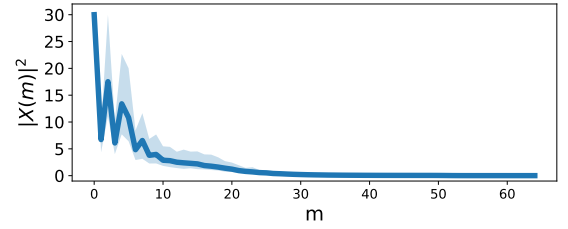


Figure 4: Take the UCIHAR dataset as an example, the energy in the frequency domain $E = \frac{1}{L} \sum_{m=0}^{L-1} |X(m)|^2$ is mostly concentrated in a compact set of frequency components, whose frequency are the ten lowest. The solid line represents the average energy for the frequency components in the UCIHAR dataset, and the shaded area indicates the range.

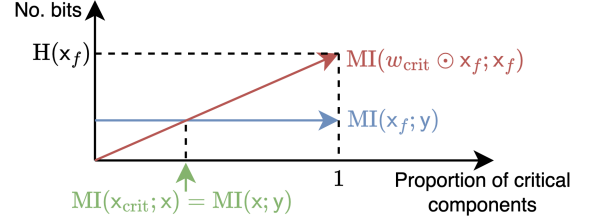


Figure 5: We aim to achieve the intersection point pointed by the green arrow where $\text{MI}(\mathbf{x}_{\text{crit}}; \mathbf{x}) = \text{MI}(\mathbf{x}; \mathbf{y})$, meaning the critical frequency components keep and only keep the semantically relevant information. The linearity of $\text{MI}(\mathbf{w}_{\text{crit}} \odot \mathbf{x}_f; \mathbf{x}_f)$ is for illustration purposes only.

this baseline as InfoMin⁺. For other baselines, we adopt the results from [15, 41] if they are available. Otherwise, we use the publicly available implementation and fine-tune the model as suggested in the original papers.

Fully-convolutional Network (FCN) [31] with an output dimension 128 is adopted as the encoder f_θ . The batch size is selected from {256, 128, 64, 32, 16, 5} according to the scale of the dataset, and the maximum training epoch is set to 200 for all the experiments. The learning rate is selected from {0.03, 0.01, 0.003, 0.001}. We adopt SGD optimizer to train the contrastive model and Adam optimizer for s. For the hyper-parameter setting, we select discretization temperature τ_w from {0.1, 0.2}, and fix temperature coefficient τ to be 0.2. λ is searched from {0.1, 0.3, 1, 3, 10, 30}. The projector g_ϕ is a two-layer MLP, with hidden and output dimensions 128.

To evaluate the performance, we employ the commonly used linear evaluation protocol. We first jointly train FrErA and the contrastive learning model, then we discard other components and keep only the pre-trained encoder f_{θ^*} frozen and train a linear classifier on top of it, as illustrated in the lower right corner of Figure 2. For time series classification tasks, we record the best accuracy (ACC) as the evaluation metric. For anomaly detection tasks, we record both the best accuracy and the Macro-F1 score.

A.5 Additional Analysis for The Main Result on Time Series Classification Tasks

From Table 1, Table 8, and Table 9, we conclude that frequency-domain augmentations outrun time-domain augmentations in general. This endorses our motivation that the frequency perspective

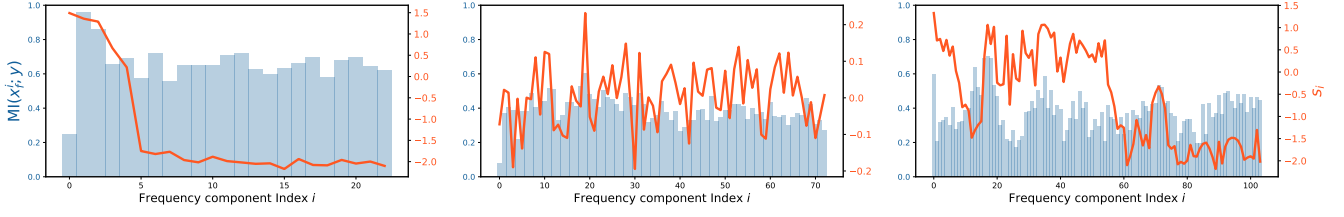


Figure 6: Despite the diverse distributions of global semantics across three datasets (Libras, ArticularWordRecognition, and Epilepsy), as shown in the blue-grey bar plots, the learned vector s , represented by the orange lines, consistently captures the inherent critical information by assigning higher values to the most semantically relevant frequency components (those of high values in the bar plots).

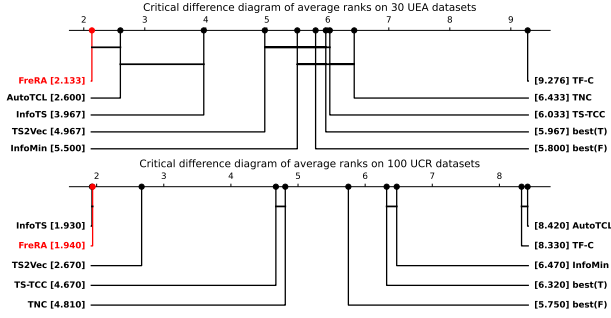


Figure 7: Critical difference diagrams on UEA and UCR archives.

Table 6: The performance of applying different statistical information to select unimportant components.

Dataset	mean (ours)	median	mean+std
UIC HAR	0.975	0.971	0.972
MS	0.982	0.976	0.975
WISDM	0.972	0.963	0.963

is superior to its time-domain counterpart in preserving global semantics. InfoMin⁺ exceeds other baselines on the three large HAR datasets, which demonstrates the efficacy of its objective. However, the performance gap between InfoMin⁺ and ours indicates that directly applying an adversarial objective in the frequency domain is not customized for our approach and causes conflict in representation learning. On the other hand, our specially designed objective better suits the frequency-domain refinement. The 5 SOTA time-series contrastive learning frameworks with carefully designed architectures and objectives become uncompetitive compared to FreRA.

It is worth noting that our datasets cover multiple applications, diverse data scales, and various types of sensor modalities. Notably, FreRA receives the best overall performance on them, which proves that our approach provides a unified view generation approach and can be flexibly applied to various time-series applications.

A.6 Ablation Studies

Effect of Unimportant Component Selection Mechanisms.

To evaluate how the choice of statistical measurement in D affects

Table 7: The performance of the selected sets of 5 frequency-domain augmentations on the three HAR datasets. The best performance is highlighted in bold, and the second-best performance is underlined.

Dataset	FreRA (ours)	lpf	hpf	p_shift	ap_p	ap_f
UIC HAR	0.975	0.921	0.939	0.958	0.959	<u>0.960</u>
MS	0.982	0.934	0.838	<u>0.970</u>	0.901	0.952
WISDM	0.972	0.934	0.800	0.943	0.865	<u>0.950</u>

the final results, we conduct an ablation study comparing the performances when using mean, median, and mean+std of vector s as the threshold. The results are shown in Table 6. All the choices outperform the baseline performances in Table 1 and the mean value achieves the best performance among them.

Vector s Captures the Inherent Semantic Distribution in the Frequency Domain. To verify the effectiveness of FreRA, in Figure 6, we visualize the learned parameter vector s , as compared to the ground truth semantics distribution in the frequency domain, on three datasets, including Libras, ArticularWordRecognition, and Epilepsy. Specifically, we use the mutual information (MI) between the frequency components with the label to quantify the ground truth importance of frequency components and presented by blue-grey bar plots. The distribution of important frequency components varies across datasets. The important components are distributed in low frequencies, middle frequencies, and across multiple frequencies in these datasets, respectively. The learned vector s which determines the importance scores of all the frequency components is presented with the orange line plots. Despite diverse distributions, s consistently captures the inherent critical information by learning to assign higher values to the most semantically relevant frequency components.

A.7 Additional Results

Full results of multivariate time series classification on the UEA archive and univariate time series classification on the UCR archive are presented in Table 9 and Table 8. The full result of the commonly used sets of 11 time-domain augmentations and 5 frequency-domain augmentations on the 3 HAR datasets are shown in Table 10 and Table 7, respectively.

Table 8: The overall classification result of 100 univariate time series datasets from the UCR archive. The best performance is highlighted in bold.

Dataset	FreRA (Ours)	best(T)	best(F)	InfoMin	InfoTS	AutoTCL	TS2Vec	TNC	TS-TCC	TF-C
ACSF1	0.760	0.660	0.470	0.580	0.850	0.480	0.910	0.730	0.730	0.100
AllGestureWiimoteX	0.707	0.526	0.561	0.549	0.630	0.517	0.777	0.703	0.697	0.100
AllGestureWiimoteY	0.746	0.620	0.601	0.611	0.686	0.624	0.793	0.699	0.741	0.100
AllGestureWiimoteZ	0.707	0.581	0.573	0.577	0.629	0.576	0.770	0.646	0.689	0.100
BeetleFly	1.000	0.700	0.900	0.800	0.950	0.650	0.900	0.850	0.800	0.450
BirdChicken	1.000	0.750	0.850	0.800	0.900	0.550	0.800	0.750	0.650	0.500
BME	1.000	0.920	0.940	0.967	1.000	0.640	0.993	0.973	0.933	0.630
CBF	1.000	0.997	0.957	0.967	0.999	0.707	1.000	0.983	0.998	0.686
Chinatown	0.988	0.910	0.886	0.939	0.988	0.983	0.968	0.977	0.983	0.904
CinCECGTorso	0.968	0.912	0.968	0.914	0.928	0.305	0.827	0.669	0.671	0.248
Coffee	1.000	0.964	0.964	1.000	1.000	0.750	1.000	1.000	1.000	0.464
Computers	0.776	0.684	0.700	0.676	0.748	0.468	0.660	0.684	0.704	0.644
Crop	0.755	0.569	0.566	0.561	0.766	0.608	0.756	0.738	0.742	0.632
DiatomSizeReduction	0.980	0.817	0.948	0.905	0.997	0.676	0.987	0.993	0.977	0.301
DistalPhalanxOutlineAgeGroup	0.799	0.655	0.755	0.645	0.763	0.640	0.727	0.741	0.755	0.732
DistalPhalanxOutlineCorrect	0.804	0.627	0.670	0.734	0.801	0.583	0.775	0.754	0.754	0.683
DistalPhalanxTW	0.755	0.676	0.719	0.669	0.727	0.597	0.698	0.669	0.676	0.669
DodgerLoopDay	0.600	0.275	0.325	0.388	0.675	0.338	0.562	-	-	0.150
DodgerLoopGame	0.942	0.833	0.797	0.855	0.942	0.725	0.841	-	-	0.522
DodgerLoopWeekend	0.993	0.935	0.949	0.978	0.986	0.920	0.964	-	-	0.739
Earthquakes	0.820	0.748	0.748	0.748	0.821	0.748	0.748	0.748	0.748	0.748
ECG200	0.890	0.830	0.840	0.800	0.930	0.700	0.920	0.830	0.880	0.940
ECG5000	0.948	0.935	0.940	0.926	0.945	0.900	0.935	0.937	0.941	0.938
ECGFiveDays	1.000	0.998	0.987	0.990	1.000	0.821	1.000	0.999	0.878	0.972
ElectricDevices	0.657	0.609	0.599	0.609	0.702	0.562	0.721	0.700	0.686	0.560
EOGHorizontalSignal	0.597	0.434	0.508	0.470	0.572	0.293	0.544	0.442	0.401	0.083
EOGVerticalSignal	0.489	0.320	0.423	0.312	0.459	0.290	0.503	0.392	0.376	0.144
FaceAll	0.888	0.628	0.728	0.658	0.929	0.689	0.805	0.766	0.813	0.714
FaceFour	0.864	0.773	0.773	0.773	0.818	0.205	0.932	0.659	0.773	0.330
FacesUCR	0.866	0.861	0.794	0.760	0.913	0.544	0.930	0.789	0.863	0.779
FordA	0.943	0.905	0.902	0.917	0.915	0.494	0.948	0.902	0.930	0.537
FordB	0.832	0.775	0.794	0.780	0.785	0.493	0.807	0.733	0.815	0.474
FreezerRegularTrain	0.994	0.804	0.856	0.820	0.996	0.717	0.986	0.991	0.989	0.742
FreezerSmallTrain	0.988	0.787	0.735	0.811	0.988	0.721	0.894	0.982	0.979	0.501
Fungi	0.941	0.667	0.667	0.677	0.946	0.263	0.962	0.527	0.753	0.860
GestureMidAirD1	0.638	0.315	0.431	0.308	0.592	0.423	0.631	0.431	0.369	0.038
GestureMidAirD2	0.608	0.292	0.138	0.269	0.492	0.177	0.515	0.362	0.254	0.038
GesturePebbleZ1	0.779	0.581	0.610	0.506	0.802	0.650	0.930	0.378	0.395	0.163
GesturePebbleZ2	0.722	0.614	0.551	0.475	0.842	0.424	0.873	0.316	0.430	0.152
GunPoint	1.000	0.887	0.993	0.933	1.000	0.800	0.987	0.967	0.993	0.573
GunPointAgeSpan	0.984	0.921	0.908	0.908	1.000	0.639	0.994	0.984	0.994	0.927
GunPointMaleVersusFemale	1.000	0.835	0.839	0.832	1.000	0.718	1.000	0.994	0.997	0.987
GunPointOldVersusYoung	1.000	1.000	1.000	1.000	1.000	0.981	1.000	1.000	1.000	1.000
Ham	0.810	0.790	0.705	0.686	0.838	0.533	0.724	0.752	0.743	0.752
HandOutlines	0.900	0.876	0.886	0.881	0.946	0.662	0.930	0.930	0.724	0.641
Haptics	0.487	0.471	0.487	0.406	0.546	0.334	0.536	0.474	0.396	0.208
Herring	0.703	0.594	0.609	0.594	0.656	0.594	0.641	0.594	0.594	0.594
HouseTwenty	0.983	0.891	0.706	0.681	0.924	0.655	0.941	0.782	0.790	0.571
InlineSkate	0.353	0.258	0.318	0.242	0.424	0.193	0.415	0.378	0.347	0.155
InsectEPGRegularTrain	1.000	1.000	1.000	1.000	1.000	1.000	1.000	1.000	1.000	1.000
InsectEPGSmallTrain	1.000	1.000	0.451	1.000	1.000	1.000	1.000	1.000	1.000	0.474
ItalyPowerDemand	0.976	0.968	0.956	0.969	0.966	0.614	0.961	0.928	0.955	0.934
LargeKitchenAppliances	0.848	0.787	0.784	0.776	0.853	0.416	0.875	0.776	0.848	0.389
Lightning2	0.951	0.672	0.721	0.721	0.934	0.639	0.869	0.869	0.836	0.738
Lightning7	0.840	0.726	0.767	0.712	0.877	0.342	0.863	0.767	0.685	0.616
Mallat	0.954	0.820	0.907	0.722	0.974	0.412	0.915	0.871	0.922	0.123
Meat	0.917	0.333	0.774	0.333	0.967	0.583	0.967	0.917	0.883	0.333
MiddlePhalanxOutlineAgeGroup	0.669	0.610	0.617	0.597	0.662	0.577	0.636	0.643	0.630	0.578
MiddlePhalanxOutlineCorrect	0.842	0.570	0.704	0.570	0.859	0.500	0.838	0.818	0.818	0.653
MiddlePhalanxTW	0.630	0.558	0.578	0.571	0.617	0.552	0.591	0.571	0.610	0.558

Dataset	FreRA (Ours)	best(T)	best(F)	InfoMin	InfoTS	AutoTCL	TS2Vec	TNC	TS-TCC	TF-C
MixedShapesRegularTrain	0.925	0.878	0.927	0.829	0.935	0.624	0.922	0.911	0.855	0.400
MixedShapesSmallTrain	0.852	0.822	0.842	0.776	0.887	0.525	0.881	0.813	0.735	0.181
MoteStrain	0.891	0.904	0.806	0.849	0.873	0.676	0.863	0.825	0.843	0.815
OliveOil	0.800	0.400	0.752	0.400	0.933	0.600	0.900	0.833	0.800	0.400
OSULeaf	0.909	0.678	0.705	0.554	0.760	0.384	0.876	0.723	0.723	0.467
Phoneme	0.273	0.211	0.200	0.208	0.281	0.158	0.312	0.180	0.242	0.104
PickupGestureWimoteZ	0.860	0.740	0.399	0.680	0.820	0.640	0.820	0.620	0.600	0.100
PigCVP	0.611	0.303	0.667	0.207	0.653	0.130	0.870	0.649	0.615	0.019
PLAID	0.523	0.330	0.269	0.307	0.355	0.451	0.561	0.495	0.445	0.061
Plane	1.000	1.000	1.000	1.000	1.000	1.000	1.000	1.000	1.000	0.952
PowerCons	0.994	0.939	0.933	0.917	1.000	0.861	0.972	0.933	0.961	0.894
ProximalPhalanxOutlineAgeGroup	0.888	0.854	0.883	0.873	0.883	0.715	0.844	0.854	0.839	0.849
ProximalPhalanxOutlineCorrect	0.893	0.722	0.784	0.698	0.927	0.820	0.900	0.866	0.873	0.801
ProximalPhalanxTW	0.849	0.678	0.800	0.780	0.844	0.771	0.824	0.810	0.800	0.795
RefrigerationDevices	0.597	0.549	0.533	0.501	0.624	0.360	0.589	0.565	0.563	0.299
Rock	0.700	0.480	0.480	0.500	0.760	0.400	0.700	0.580	0.600	0.280
ScreenType	0.491	0.368	0.656	0.421	0.493	0.355	0.411	0.509	0.419	0.344
ShakeGestureWimoteZ	0.980	0.840	0.800	0.840	0.920	0.787	0.940	0.820	0.860	0.100
ShapeletSim	1.000	1.000	0.978	1.000	0.856	0.533	1.000	0.589	0.683	0.467
ShapesAll	0.822	0.368	0.627	0.415	0.852	0.802	0.905	0.788	0.773	0.582
SmoothSubspace	0.987	0.873	0.893	0.860	1.000	0.913	0.993	0.913	0.953	0.653
SonyAIBORobotSurface2	0.957	0.815	0.867	0.807	0.953	0.769	0.890	0.834	0.907	0.846
SonyAIBORobotSurface1	0.953	0.885	0.906	0.854	0.927	0.778	0.903	0.804	0.899	0.804
StarLightCurves	0.973	0.874	0.964	0.891	0.973	0.849	0.971	0.968	0.967	0.855
Strawberry	0.965	0.835	0.876	0.849	0.978	0.614	0.965	0.951	0.965	0.832
SwedishLeaf	0.950	0.789	0.874	0.787	0.950	0.794	0.942	0.880	0.923	0.891
Symbols	0.980	0.912	0.943	0.847	0.979	0.699	0.976	0.885	0.916	0.174
SyntheticControl	1.000	0.990	0.980	0.997	1.000	0.880	0.997	1.000	0.990	0.760
ToeSegmentation1	0.961	0.943	0.921	0.939	0.934	0.496	0.947	0.864	0.930	0.570
ToeSegmentation2	0.931	0.815	0.800	0.869	0.915	0.692	0.915	0.831	0.877	0.338
Trace	1.000	0.880	1.000	0.920	1.000	0.650	1.000	1.000	1.000	0.690
TwoLeadECG	0.987	0.867	0.984	0.901	0.998	0.565	0.987	0.993	0.976	0.921
TwoPatterns	1.000	0.997	0.999	0.957	1.000	0.264	1.000	1.000	0.999	0.654
UMD	1.000	0.938	0.617	0.979	1.000	0.590	1.000	0.993	0.986	0.778
Wafer	0.996	0.960	0.956	0.959	0.998	0.921	0.998	0.994	0.994	0.994
Wine	0.833	0.500	0.500	0.500	0.963	0.500	0.889	0.759	0.778	0.500
WordSynonyms	0.619	0.350	0.384	0.359	0.704	0.497	0.704	0.630	0.531	0.487
Worms	0.792	0.558	0.636	0.623	0.753	0.403	0.701	0.623	0.753	0.429
WormsTwoClass	0.831	0.753	0.714	0.714	0.857	0.558	0.805	0.727	0.753	0.584
Yoga	0.808	0.693	0.699	0.607	0.869	0.536	0.887	0.812	0.791	0.688
Avg. ACC	0.850	0.723	0.744	0.718	0.849	0.598	0.845	0.776	0.780	0.542
Avg. RANK	1.940	6.320	5.750	6.470	1.930	8.420	2.670	4.810	4.670	8.330

Table 9: The overall classification result of 30 multivariate time series datasets from the UEA archive. The best performance is highlighted in bold.

Dataset	FreRA (ours)	best(T)	best(F)	InfoMin	InfoTS	AutoTCL	TS2Vec	TNC	TS-TCC	TF-C
Articulatory WordRecognition	0.990	0.887	0.947	0.913	0.987	0.983	0.987	0.973	0.953	0.467
AtrialFibrillation	0.467	0.400	0.333	0.267	0.200	0.467	0.200	0.133	0.267	0.040
BasicMotions	1.000	1.000	1.000	1.000	0.975	1.000	0.975	0.975	1.000	0.475
CharacterTrajectories	0.991	0.953	0.976	0.990	0.974	0.976	0.995	0.967	0.985	0.090
Cricket	1.000	0.986	0.986	0.958	0.986	1.000	0.972	0.958	0.917	0.125
DuckDuckGeese	0.760	0.660	0.660	0.700	0.540	0.700	0.680	0.460	0.380	0.340
Eigen Worms	0.863	0.779	0.840	0.794	0.733	0.901	0.847	0.840	0.779	-
Epilepsy	0.993	0.906	0.935	0.920	0.971	0.978	0.964	0.957	0.957	0.217
ERing	0.919	0.885	0.907	0.904	0.949	0.944	0.874	0.852	0.904	0.167
EthanolConcentration	0.323	0.297	0.262	0.243	0.281	0.354	0.308	0.297	0.285	0.247
FaceDetection	0.581	0.564	0.521	0.560	0.534	0.581	0.501	0.536	0.544	0.502
FingerMovements	0.610	0.530	0.500	0.500	0.630	0.640	0.480	0.470	0.460	0.510
HandMovementDirection	0.514	0.378	0.365	0.324	0.392	0.432	0.338	0.324	0.243	0.405
Handwriting	0.593	0.501	0.469	0.569	0.452	0.384	0.515	0.249	0.498	0.051
Heartbeat	0.785	0.741	0.746	0.737	0.722	0.785	0.683	0.746	0.751	0.737
Japanese Vowels	0.965	0.938	0.938	0.938	0.984	0.984	0.984	0.978	0.930	0.135
Libras	0.911	0.761	0.822	0.800	0.883	0.833	0.867	0.817	0.822	0.067
LSST	0.494	0.393	0.391	0.473	0.591	0.554	0.537	0.595	0.474	0.314
MotorImagery	0.550	0.530	0.540	0.530	0.630	0.570	0.510	0.500	0.610	0.500
NATOPS	0.900	0.867	0.872	0.822	0.933	0.944	0.928	0.911	0.822	0.533
PEMS-SF	0.746	0.653	0.671	0.699	0.751	0.838	0.682	0.699	0.734	0.312
PenDigits	0.973	0.946	0.946	0.970	0.990	0.984	0.989	0.979	0.974	0.236
PhonemeSpectra	0.274	0.226	0.226	0.240	0.249	0.218	0.233	0.207	0.252	0.026
RacketSports	0.888	0.816	0.796	0.822	0.855	0.914	0.855	0.776	0.816	0.480
SelfRegulationSCP1	0.908	0.836	0.870	0.867	0.874	0.891	0.812	0.799	0.823	0.502
SelfRegulationSCP2	0.622	0.589	0.594	0.622	0.578	0.578	0.578	0.550	0.533	0.500
SpokenArabicDigits	0.984	0.935	0.871	0.981	0.947	0.925	0.932	0.934	0.970	0.100
StandWalkJump	0.667	0.400	0.333	0.333	0.467	0.533	0.467	0.400	0.333	0.333
UWaveGestureLibrary	0.900	0.794	0.800	0.872	0.884	0.893	0.884	0.759	0.753	0.125
InsectWingbeat	0.462	0.363	0.456	0.443	0.470	0.488	0.466	0.469	0.264	0.108
Avg. ACC	0.754	0.684	0.686	0.693	0.714	0.742	0.704	0.670	0.668	0.298
Avg. RANK	2.133	5.967	5.800	5.500	3.967	2.600	4.967	6.433	6.033	9.276

Table 10: The performance of the selected sets of 11 time-domain augmentations on the three HAR datasets. The best performance is highlighted in bold, and the second-best performance is underlined. ‘t_flip’, ‘t_warp’, ‘perm_jit’ and ‘jit_scal’ are short for time-flipping, time-warping, permutation-and-jitter and jitter-and-scale.

Dataset	FreRA (ours)	jit	scale	negation	perm	shuffling	t_flip	t_warp	resample	rotation	perm_jit	jit_scal
UCIHAR	0.975	0.958	0.940	0.892	0.910	0.913	0.917	0.934	0.947	0.596	<u>0.959</u>	0.945
MS	0.982	0.930	0.914	0.813	0.927	0.910	0.915	0.925	<u>0.956</u>	0.887	<u>0.948</u>	0.915
WISDM	0.972	<u>0.942</u>	0.928	0.901	0.932	0.925	0.884	0.910	<u>0.942</u>	0.872	0.932	0.927